Clays and Clay Minerals, Vol. 59, No. 6, 640–653, 2011.

HYDRATION BEHAVIOR OF MX80 BENTONITE IN A CONFINED-VOLUME SYSTEM: IMPLICATIONS FOR BACKFILL DESIGN

JULIA N. PERDRIAL[1,2,*] AND LAURENCE N. WARR[3]

[1] Centre de Géochimie de la Surface, CNRS & Université Louis Pasteur, 1 rue Blessig, 67084 Strasbourg, France
[2] Department of Soil, Water and Environmental Science, University of Arizona, Tucson, AZ 85721, USA
[3] Institut für Geographie und Geologie, Ernst-Moritz-Arndt Universität, F. Ludwig-Jahn-Str. 17A, 17487 Greifswald, Germany

Abstract—Bentonites are considered suitable backfill material for planned underground nuclear-waste repositories because of an inherent capacity to self-seal and retain contaminants when hydrated. Barrier effectiveness, however, depends on the physical properties of bentonite after placement in a repository site, where hydration state and bulk density can vary. The objective of the present study was to investigate commercial bentonite MX80 hydration rates and mechanisms during water infiltration into dry, moist, and wet samples using the 'wet-cell' X-ray diffraction technique. During experimentation, water enters a small flow-through cell and induces swelling within a confined reaction volume, analogous to clay barriers in excavated underground sites. Results demonstrated the importance of using dry, well compacted (>1.4 g/cm^3) bentonite, which became saturated slowly (<2.0×10^{-9} m/s) with minimal water in non-interlayer sites (external-surface sites, or within pores). The significant degree of interlayer expansion dominated by the formation of two and eventually three water layers developed as hydration clusters with greater probabilities for the same thickness to lie in adjacent interlayer sites. The relatively thicker particles and the less accessible surface area of hydrated, initially dry bentonite probably resulted in less pore-controlled diffusion, but also less potential radionuclide adsorption by surface complexation. Moist MX80 had the greatest water uptake, the smallest (1.23 g/cm^3) dry bulk density, and the greatest proportion of water in pores and on external surfaces. Water that initially accumulated in pore spaces subsequently acted as a reservoir for interlayer hydration and probable gel formation in trapped voids, which is expected to occur in more loosely filled gaps within an excavated repository.

Key Words—Bentonite Hydration, Confined Volume, Laboratory Analogue, Nuclear Waste Disposal.

INTRODUCTION

One of the most studied properties of smectite clay minerals is the ability to adsorb large quantities of water and other polar substances by the ordered expansion of the crystal lattice (Hofman and Bilke, 1936; Mooney *et al.*, 1952; MacEwan and Wilson, 1980; Sposito and Prost, 1982; Bergaya and Lagaly, 2006). Key to this property is a structure built of a succession of tetrahedral-octahedral-tetrahedral 2:1 units with negative interlayer surface charges due to isomorphous substitutions balanced by exchangeable cations. During cation hydration, water molecules arrange into well defined layers (up to four) within the smectite interlayer space (Bailey, 1980).

In order to monitor the degree of interlayer expansion during hydration, a common approach is to study smectite hydration states by varying the relative humidity in combination with X-ray diffraction (XRD) measurements (Mooney *et al.*, 1952; Collins *et al.*, 1992; Kühnel and van der Gaast, 1993; Chipera *et al.*, 1997; Ferrage *et al.*, 2005) or bulk-volume measurements (Likos, 2004). Under such conditions, the amount of water that is incorporated within the interlayer spaces has been studied and quantified successfully based on water-vapor adsorption-desorption isotherms (Kraehenbuehl *et al.*, 1987; Kahr *et al.*, 1990; Bérend *et al.*, 1995; Cases *et al.*, 1997).

A number of studies have investigated the free expansion of smectite particles in water and aqueous electrolyte solutions (Norrish, 1954; Norrish and Quirk, 1954; Schramm and Kwak, 1982; Laird *et al.*, 1995; Wilson *et al.*, 2004). Under these conditions, non-interlayer water might be loosely bound to external particle surfaces or be present as free water within pores between particles and aggregates (Prost, 1975; Sposito and Prost, 1982; Kaufhold *et al.*, 2010; Likos and Wayllace, 2010). In free-swelling systems, the proportion of water in external pores can increase dramatically during hydration, such as in Na-bentonites fully dispersed in low ionic-strength solutions. Osmotic pressure can expand interlayers, split particles, and make interlayer surfaces more accessible (Lagaly, 1993, 2006; Salles *et al.*, 2009). The specific surface areas (SSA) of bentonite powder (external surface area) can be measured by fitting nitrogen adsorption data to the Brunauer-Emmet-Teller (BET) equation and the pore-size distribution can be measured using the Hg-injection technique (Olson, 1985; Delage and Schanz, 2007).

* E-mail address of corresponding author:
jnperdri@email.arizona.edu
DOI: 10.1346/CCMN.2011.0590609

Bentonite swelling behavior in confined reaction volumes has also been studied under conditions that are analogous to underground waste repositories (Villar, 2007; Warr and Berger, 2007).

Confined volumes result from the limited space between encased waste material, sealed wall rock, and within joints and open fissures. Bentonite barrier construction within this confined space forms a key part of the multi-barrier concept, which is intended to limit aqueous fluid penetration and circulation within the repository core. As a result, experimental quantification of water incorporation rates and mechanisms within the bentonite seal is of major importance. The different water storage sites (interlayers, external surfaces, and pores) influence sealing mechanisms, adsorption, and transport in notably different ways. Diffusive transport of radioactive cationic species could occur in water-filled voids (pore-water diffusion), along particle surfaces, or most slowly through interlayers. Anionic species should be excluded from interlayers and charged surfaces (Donnan effect) and diffusive anion transport should be largely dependent on available pore space (Pusch, 2006a).

The SSA is an important bentonite seal property which controls surface phenomena and uptake of organic and inorganic molecules (Michot and Villieras, 2006). As the accessible-surface-area increases during particle expansion, theoretical SSA values of 850 m^2/g can be reached (Michot and Villieras, 2006). However, particles cannot expand freely under confined-volume conditions and accessible-surface-area increases will be more limited. Direct measurements of changes in accessible surface area during hydration are difficult to obtain under experimental conditions and are generally not well constrained.

In order to investigate the essential parameters of bentonite performance, large-scale *in situ* experiments have been developed, such as the mock-up experiment in Sweden and the Czech Republic or the 'FEBEX' (Full-scale Engineered Barriers EXperiment) of Switzerland (Lloret and Villar, 2007; Pusch *et al.*, 2007; Villar and Lloret, 2007). The tests are (almost) full scale and bentonite buffer performance can be studied under waste-repository-relevant conditions. Several types of bentonite material are in use, such as high-density pellets (Hoffmann *et al.*, 2007), pellet/powder mixtures (Imbert and Villar, 2006), or highly compressed blocks (Johannesson *et al.*, 1995). In order to induce swelling and achieve the desired sealing of the bentonite buffer, the system can be irrigated and, in the case of compressed blocks, a system of gaps and joints will exist (Gattermann *et al.*, 2001). Whereas compacted blocks and pellets will achieve dry densities of up to 2 g/cm^3 (Gattermann *et al.*, 2001; Pusch, 2006b; Hoffmann *et al.*, 2007), densities in interfacial areas within pellet mixtures and between blocks and/or the host-rock formation will be lower (Stroes-Gascoyne *et al.*, 2008; Perdrial *et al.*, 2009) and result in a different hydro-mechanical behavior.

Another approach used to study bentonite hydration under confined-volume conditions is to construct small-scale laboratory analogues that only simulate selected parameters, but are significantly cheaper, require less preparation, and can be monitored more easily. In the present study, a number of reaction-cell ("wet-cell"; Warr and Hoffman, 2003) experiments were conducted which allowed *in situ* measurements of bentonite hydration by XRD techniques. Various bulk densities could be studied during aqueous solution infiltration which simulated irrigation events. In combination with peak calculations (*CALCMIX*, Plançon and Drits (1999)), it was possible to (1) obtain kinetics information on water uptake, (2) quantify water distribution in the different compacted-bentonite water-storage sites, and (3) gain important qualitative information on interlayer-water ordering within smectite particles and determine accessible-surface-area changes during hydration. The experimental results are discussed in terms of the hydration mechanisms at different scales from clay lattice layer to bulk bentonite for dry and moist MX80 hydration states with varying bulk densities, compared to a previous study on wet MX80 (Perdrial *et al.*, 2009).

MATERIALS AND METHODS

MX80 bentonite and infiltrating water

MX80 is a bentonite sold commercially by 'CETCO France' and was chosen for this study as an example of a possible future backfill material (ANDRA, 2005). A sample was obtained from the manufacturer as raw material and was used without further purification or cation exchange treatment. The type of smectite is montmorillonite, which comprises ~76% of the bulk raw material. Interlayers are heteroionically occupied by Na^+ and Ca^{2+} according to the formula (Sauzeat *et al.*, 2001):

$$Na_{0.18}Ca_{0.11}[Al_{1.52}Mg_{0.26}Fe(III)_{0.17}][Si_{3.96}Al_{0.04}]O_{10}(OH)_2$$

The remaining mineral fraction (Table 1) consists of mica, feldspar, quartz, calcite, and pyrite. As the present study focused on the hydration behavior of the montmorillonite, the role of non-swelling accessory minerals was not taken into account. To avoid complications with cation exchange reactions, deionized water (18.2 MΩ-cm) was used as the infiltrating solution, as opposed to the natural ground- and sea-water solutions previously investigated using this type of reaction cell (Warr and Berger, 2007).

Reaction-cell X-ray diffractometry

The reaction-cell device was described in detail by Warr and Hofmann (2003), Warr and Berger (2007), and Perdrial *et al.*, 2009) so only a brief description is provided here. The reaction cell consists of a small

https://doi.org/10.1346/CCMN.2011.0590609 Published online by Cambridge University Press

Table 1. Characteristics of the MX80 bentonite used in the experiments.

Characteristics of smectite				
Amount of smectite (%)	Interlayer cation	CEC (meq/100 g)	Surface area (m^2/g)	Layer charge (eq/$(Si,Al)_4O_{10}$)
~76% montmorillonite	Na, Ca	69.6	30.03	0.28
Accessory minerals (%)				
Mica	Feldspar	Quartz	Calcite	Pyrite
2.8–3.8	4.5	5–6	0.3–1.4	0.5

Data from Sauzeat *et al*. (2001)

disc-shaped Teflon reaction chamber 24 mm in diameter and 7.7 mm deep (volume = 3.5 cm^3). Bentonite powder was packed into the chamber with a brass rod which imparted a rough texture parallel to the sample-holder surface. The reaction cell was sealed using a thin X-ray transparent Kapton© film held in place with a Teflon© o-ring seal (Figure 1a). A pressure cap was screwed onto the top of the cell (Figure 1b) to maintain a constant reaction volume during experiments. About 200 mL of solution was placed in an 8 cm tall Teflon© bottle that was screwed directly onto the cell to allow inflow (Figure 1c). Filters placed across holes within the reaction cell prevented powder loss from the chamber. However, the material swells and seals itself during experiments and neither solution nor solid-material losses from the reaction cell were observed.

The pressure cap was removed for XRD measurement (20–45 min, Figure 1d). During this time no swelling was observed to change the height of the sample. Repeated measurements were made at selected intervals throughout the experiment, enabling sequential XRD patterns to be plotted against time. Measurement frequency was adjusted according to the observed rate of reaction and evaporation was minimized by the Kapton© film.

Bentonite powder samples with three different water contents and bulk densities were used (Table 2). The sample with the smallest amount of initial water (dry MX80, $w_{initial}$ = 0.01 mL/g, including interlayer water) had a total bulk density of 1.43 g/cm^3 (ϕ_{total}). Excluding all water, this corresponds to a dry bulk density (ϕ_{dry}) of 1.41 g/cm^3 (Table 2). A sample with intermediate initial water content (moist MX80) contained 0.09 mL/g of water and had smaller bulk densities of ϕ_{total} = 1.35 g/cm^3 and ϕ_{dry} = 1.23 g/cm^3.

The wet MX80 data were taken from Perdrial *et al*. (2009), who used the same experimental setup and conditions and, therefore, comparisons were deemed valid. The greatest initial water content was 0.23 mL/g with wet and dry bulk densities = 1.60 g/cm^3 and 1.31 g/cm^3, respectively. Different initial water contents were achieved by oven-drying (110ºC) for 2 weeks (dry MX80), 5 days (moist MX80), or by adding water (wet MX80) prior to compaction.

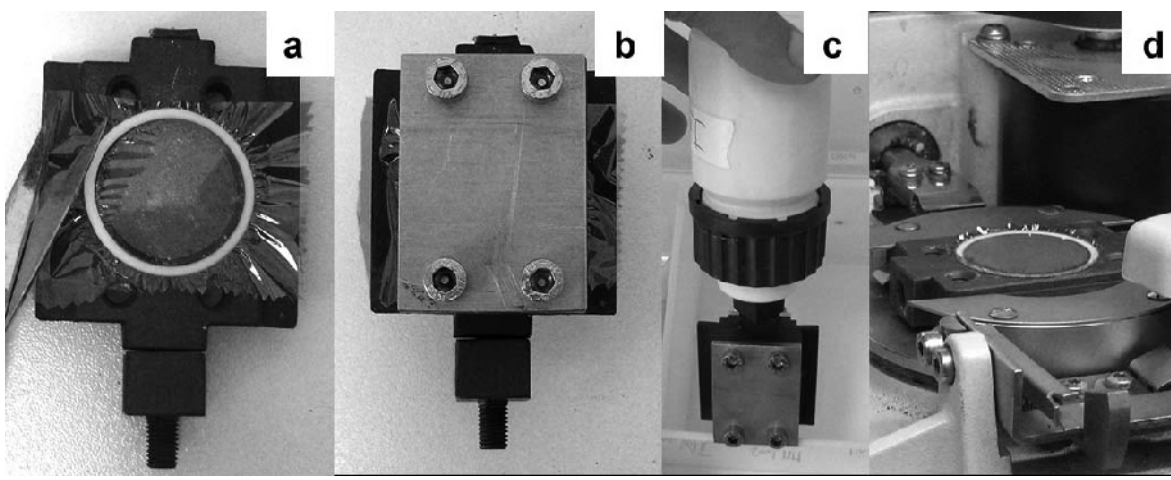

Figure 1. (a) Reaction cell containing powdered MX80 bentonite, sealed with Kapton© film. (b) Closed reaction cell with pressure cap. (c) Reaction cell with Teflon bottle providing solution. (d) Reaction cell mounted on the sample holder of the X-ray diffractometer.

https://doi.org/10.1346/CCMN.2011.0590609 Published online by Cambridge University Press

Table 2. Initial (prior to compaction) water contents of the MX80 bentonite powders and corresponding total and dry bulk densities.

Sample	Initial water content ($w_{initial}$) (mL/g)	Total bulk density (ϕ_{total}) (g/cm^3)	Dry bulk density (ϕ_{dry}) (g/cm^3)
Dry MX80	0.01	1.43	1.41
Moist MX80	0.09	1.35	1.23
Wet MX80	0.23	1.60	1.31

Data for wet MX80 from Perdrial *et al*. (2009)

X-ray diffraction

Analyses were carried out using a theta-theta Bruker Siemens D5000 diffractometer with CuKα radiation, operated under a potential of 40 kV and a beam current of 30 mA, with 1º divergent slits and a 0.15º detector slit. Scanning parameters were 0.02º2θ per step with a 10 s count time per step to obtain high-quality reflections that do not require post-measurement smoothing. Scan ranges of 2−15º2θ were used routinely to monitor shifting of the smectite 001 reflection whereas scan ranges of 2−70º2θ were used to monitor *hkl* reflections at selected intervals. Any intensity variations between measurements caused by textural changes in the sample were calibrated by normalizing the patterns to the 4.26 Å and 3.34 Å quartz reflections.

Quantifying hydration using CALCMIX

The procedure applied to quantify the hydration structure of smectite interlayers has been described previously (Warr and Berger, 2007; Perdrial *et al.*, 2009). Briefly, the water layers were quantified by comparison with calculated patterns using the *CALCMIX* software (Plançon and Drits, 1999), which calculates the theoretical diffraction patterns of mixed-layer minerals based on Méring's (1949) principle. In order to calculate mixtures of different water-layer structures, the standard mineral database was modified for montmorillonite containing 0, 1, 2, 3, and 4 water layers (WL). The relevant chemical composition and structure of the MX80 montmorillonite was entered into the program's mineral database. The average defect-free domain size (particle thickness) that best fitted the XRD profiles was selected for the given hydration state of the samples, assuming lognormal size distributions (Drits *et al.*, 1997; Drits *et al.*, 1998). The degree of ordering for mixed-layered WL structures (the Reichweite) was selected manually after the other parameters were defined. Relative WL abundances obtained from *CALCMIX* calculations were used to estimate the amount of interlayer water based on data obtained from isotherm adsorption experiments (Cases *et al.*, 1992; Bérend *et al.*, 1995; Cases *et al.*, 1997). As >2 WLs have not been observed in relative humidity experiments, the amount of water contained in 3 and 4 WL structures was extrapolated from the isotherm curves. For calculations, the following values were used: 1−WL = 0.09 mL/g, 2−WL = 0.18 mL/g, 3−WL = 0.27 mL/g, and 4−WL = 0.36 mL/g. In addition to quantifying interlayer water, the total water uptake into smectite samples during hydration was determined by monitoring gravimetrically the relative weight change of the reaction-cell apparatus during experimental runs. For this, a precision analytical balance with a standard deviation of ~0.1 mg was used. Subtraction of the calculated interlayer water from the measured total water content yielded the volumes of surface water and pore water in the samples (*i.e.* non-interlayer water: Warr and Berger, 2007; Perdrial *et al.*, 2009).

Bulk densities were calculated by dividing clay weight by wet-cell volume. Because even a dry smectite always contains a certain amount of interlayer water, dry bulk densities (devoid of interlayer water) had to be calculated. For this, interlayer water values, calculated using *CALCMIX* results for the first XRD measurement, were subtracted. For the bulk density of wet MX80, water was added prior to the experimental run and interlayer water was subtracted to yield the initial surface water and pore water (Perdrial *et al.*, 2009). Changes in particle thickness are a common feature observed during hydration (Tessier, 1990) and can be used to estimate theoretical increases in accessible surface area based on the following relationships:

$$\Delta s = (n_{initial}/n) \times 2 \quad (1)$$

and

$$SA_{calc} = 0.5 SSA_{BET} \times \Delta s \quad (2)$$

where Δs is the change in number of surfaces, $n_{initial}$ is the number of layers per particle (equivalent to stack) in the dry state, n is the number of layers per particle, SA_{calc} is the calculated corresponding surface area, and SSA_{BET} is the measured BET-N_2 surface area.

A particle thickness of 19 layers was obtained from the *CALCMIX* calculation of the first measurement of the dry MX80 sample, which was taken as the reference particle thickness ($n_{initial}$) and assumed to correspond to the measured BET-N_2 surface area of 30 m^2/g (SSA_{BET}). The method was validated by calculating a ~570 m^2/g maximum surface area for MX80 monolayer particles,

https://doi.org/10.1346/CCMN.2011.0590609 Published online by Cambridge University Press

which is close to the value of Michot and Villieras (2006) for fully dispersed montmorillonite.

Applicability to waste-repository conditions

In the present study, confined-volume conditions were simulated as an analog for an underground nuclear-waste repository. The total sample bulk density ranged between 1.35 g/cm^3 and 1.6 g/cm^3 when saturated, corresponding to dry densities between 1.23 g/cm^3 and 1.4 g/cm^3. These preparations were notably lower than the compressed bentonite blocks intended for use in a repository site (up to 2 g/cm^3) and were more equivalent to the bulk densities achieved by using pressed pellets or less compacted powder to seal interfacial regions such as gaps around the blocks. The hydration behavior of the highly compressed bentonite blocks is not addressed in the present study; further experiments are required.

Definitions

The term 'particle' was used here to describe a single smectite crystallite composed of lattice layers stacked coherently in the crystallographic *c* direction and acting as X-ray scattering domains. The terms 'particle' and 'stack' are, therefore, used interchangeably. The term 'aggregate' refers to a discrete group of two or more particles that are attached incoherently.

RESULTS AND DISCUSSION

Total water uptake

Compacted material hydration capacities were measured from the increase in weight after water uptake. Hydration capacity is largely a function of sample porosity, which is inversely dependent on bulk density. However, layer charge and exchangeable cations also affect water adsorption. Total water uptake by MX80 bentonite and a variety of other Na,Ca-smectites (Warr and Berger, 2007; Berger, 2008; Perdrial *et al.*, 2009) plotted against bulk density (Figure 2) revealed three groups of smectites, based on interlayer cation composition, and produced good correlations with *y*-axis intercepts of ~2.0–2.1 g/cm^3. This intercept corresponded to 0 mL water uptake and was close to the smectite particle density (~2.3–2.5 g/cm^3: Grim, 1962; Lagaly, 2006) which is largely independent of interlayer cation type.

Despite the common *y*-axis intercepts, linear-slope trends vary for Na-smectites and Ca-smectites and confirm interlayer cation importance in water uptake with 15% more water in Ca exchange sites. As noted by Pusch (2006a), textural differences between Na- and Ca-bentonites become more evident with decreased bulk density. The MX80 sample is a Na,Ca-bentonite and the water-uptake values are between those of homoionic Na-smectite and Ca-smectite.

Water-uptake curves for three different MX80 initial hydration states (Figure 3) show slow and continuous hydration. Water uptake by dry MX80 was almost linear and continuous until ~1490 h with 0.24 mL/g uptake at 1.6×10^{-4} mL/g/h. The rate of uptake then decreased until 5040 h with a 0.36 mL/g maximum uptake by experiment end at 7.1×10^{-5} mL/g/h. For the moist MX80 with an intermediate initial water content, a water-saturation steady state developed by 3130 h when the greatest (0.54 mL/g) rate of water absorption at 1.7×10^{-4} mL/g/h occurred. Wet MX80 had the largest (0.23 mL/g) initial water content and significantly less (0.32 mL/g) water uptake. The first (0.09 mL/g) water uptake occurred in just 1998 h whereas uptake of the remaining water into the cell occurred at a relatively slow rate (5.1×10^{-5} mL/g/h).

The slow hydration of this heteroionic (Na, Ca) MX80 showed behavior more typical of Na-bentonites as opposed to the rapid water uptake of pure Ca-bentonites (MacEwan and Wilson, 1980; Warr and Berger, 2007) and was observed in other MX80 hydration studies (Sauzeat *et al.*, 2001).

The moist MX80 sample took up most water with a total of 0.54 mL/g (Table 3) because it had the lowest bulk density and, therefore, should have the highest capacity for accommodating additional water. However, it is not the most densely packed sample (dry MX80) that incorporated the least water. Unexpectedly, the wet MX80 took in the smallest amount (0.32 mL/g), probably reflecting textural differences induced during compaction of the wet paste into the respective disc-shaped reaction cells. The wetted bentonite showed a more plastic behavior compared to dry powder samples, allowing particles and dividing pore voids to orient more

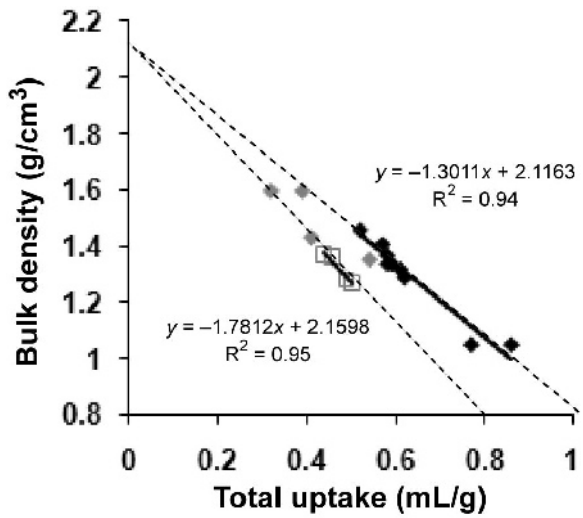

Figure 2. Correlation between bulk density and total water uptake into smectites and bentonites. Materials containing predominantly Ca in smectite interlayers (black diamonds) take in more water than the Na varieties (open gray squares). Water uptake by Na,Ca-smectite containing MX80 bentonite (gray diamonds) shows intermediate values.

https://doi.org/10.1346/CCMN.2011.0590609 Published online by Cambridge University Press

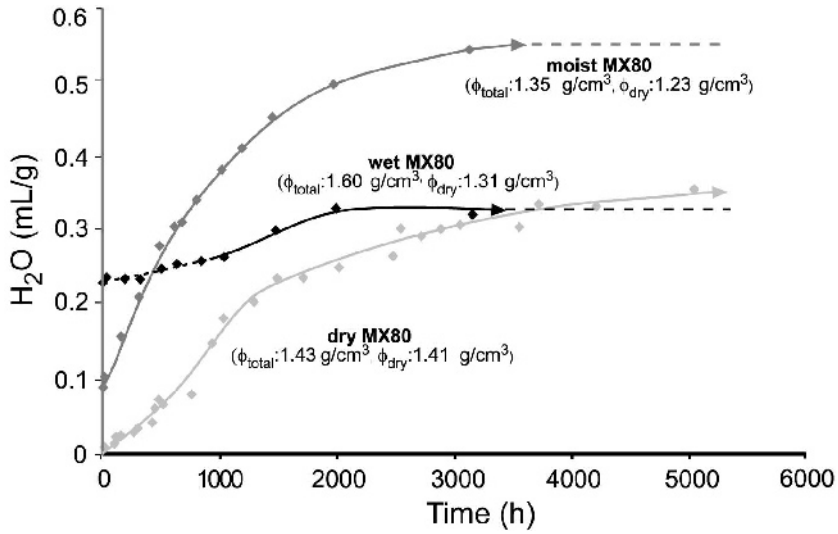

Figure 3. Total water uptake into pressed MX80 bentonite powders of different initial hydration states and bulk densities, as determined by weight gain.

parallel to the direction of water flow. The presence of such an anisotropy could partly explain the relatively short time required to reach the point of saturation (after just 2000 h) and a relative reduction in total water intake due to the effects of non-homogeneous swelling.

Dynamics of interlayer hydration

Calculated changes in water-layer abundance in MX80 samples at three different initial hydration states during hydration (Figure 4) indicated an initial water-layer abundance which contained 94% dehydrated structures (0-WL) in MX80 dry powder. Although this powder was designated as a dry powder, it contained ~6% of 1-WL prior to solution infiltration (Figure 4a). After solution uptake, 2-WL was the dominant structure in the dry powder for most of the hydration process. Hydration reached a ~70% maximum around 1030 h, which was followed by a 14% decrease by the end of the experiment. The 3-WL structure developed slowly and continuously into a dominant (78%) quasi stable-state structure with 8% 4-WL after a 3050 h hydration period.

Initially, the moist MX80 sample contained 1-WL (5%) and 2-WL (4%) before solution infiltration (Figure 4b). During the first 300 h of the experiment, all non-hydrated smectite interlayers were completely replaced by 1-WL and 2-WL structures. The 1-WL and

Table 3. Water uptake into the various storage sites of MX80 montmorillonite and calculated saturation velocities as a function of different initial hydration state.

	Dry MX80	Moist MX80	Wet MX80
Total water			
Initial amount (mL/g)	0.001	0.09	0.23
Quasi-stable state (h)	3720	3130	1998
Final content (mL/g)	0.36 (5040 h)	0.54 (3130 h)	0.32 (3150 h)
Rate (mL/g/h)	7.1×10^{-5}	1.7×10^{-4}	5×10^{-5}
Interlayer water			
Quasi-stable state (h)	3720	1449	1998
Final content (mL/g)	0.31 (5040 h)	0.36 (3130 h)	0.26 (3150 h)
Proportion (%)	86.1	67.9	81.3
External (surface and pore) water			
Quasi-stable state (h)	3720	1997	1998
Final content (mL/g)	0.05 (5040 h)	0.18 (3130 h)	0.06 (3150 h)
Proportion (%)	13.9	32.1	18.7
Saturation			
Saturation velocity (m/s)	2.0×10^{-9}	2.1×10^{-9}	3.3×10^{-9}
Saturation through 1 m (y)	17.7	14.9	9.5

https://doi.org/10.1346/CCMN.2011.0590609 Published online by Cambridge University Press

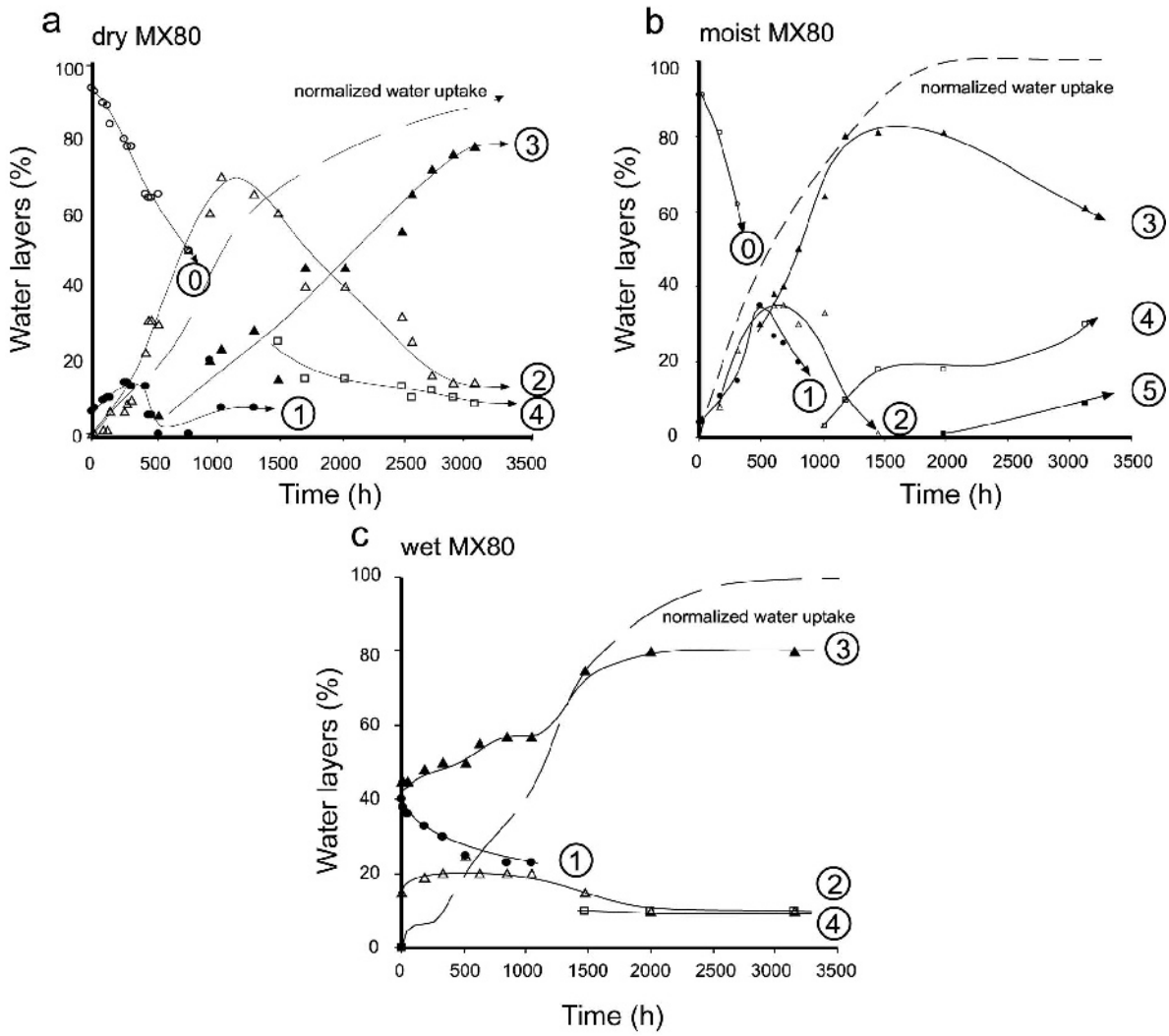

Figure 4. Development of water-layer structures in montmorillonite during hydration of MX80 bentonite, as determined by calculations using *CALCMIX* (Plançon and Drits, 1999) for dry (a), moist (b), and wet MX80 (c). Encircled numbers stand for water-layer thickness. Data for part c from Perdrial *et al.* (2009).

2-WL structures reached a maximum of 35% after 490 h for 1-WL and after 682 h for 2-WL. The 3-WL structure replaced the 1-WL and 2-WL structures relatively early and 3-WL abundance was >60% by the final stages of the experiment. The 4-WL structure was also detected and formed by replacing 2-WL and 3-WL. In addition, the broad shape of the XRD pattern at low 2θ angles (data not shown) indicated the presence of even thicker hydrated structures, which were best fitted using an assumed d_{001} of ~22.8 Å. For simplicity, this structure was referred to as a 5-WL structure, although the precise organization of the water layers was not clear. The 5-WL structure may reflect gel formation in pores that were available due to the lower bulk density. At the end of the saturation experiment, the powder apparently contained 9% of 5-WLs, 30% 4-WLs, and 61% 3-WLs.

The wet MX80 bentonite had a significantly different interlayer hydration pattern than the dehydrated (dry and moist) bentonite samples (Figure 4c, Perdrial *et al.*, 2009). Because the sample already contained a relatively large amount of water (0.23 mL/g), the initial hydration state had relatively thick water-layer structures with 40% 1-WL, 15% 2-WL, and 45% 3-WL. The subsequent water-layer development pattern was less complicated with a gradual 3-WL increase which remained the most abundant structure. This gradual increase corresponded to a gentle decrease in 1-WL and 2-WL structures, whereas ~10% of a 4-WL structure formed after 1500 h and remained unchanged until the end of the experiment. In all experiments, 3-WL structures were most abundant until the end of the experimental run.

Besides relative water-layer abundance, the XRD patterns contained statistical information on the organization of water layers within smectite particles, which can be expressed using the Reichweite (R) value calculated using *CALCMIX* software. The R value is a

https://doi.org/10.1346/CCMN.2011.0590609 Published online by Cambridge University Press

measure that describes ordering probability, which ranged from zero (R = 0) for a random WL arrangement to one (R = 1) for these XRD patterns. In a two-component system, R = 1 reflects the sum of probabilities of adjacent water layers of the same type. Values of R >1 did not appear applicable to the XRD patterns and were, therefore, not used in the calculations.

An example of the ordering probability for different WL structures formed during hydration was calculated for dry MX80 at two end-member hydration stages to show hydration effects on WL ordering (Figure 5). The probability that a dehydrated (0-WL) structure was adjacent to another 0-WL structure was always very high (p00 = 0.57 to 0.94) during the first 480 h of infiltration. Other high probability combinations were 1-WL (p10) and 2-WL (p20) structures adjacent to a 0-WL structure with both p10 and p20 values of 0.7−0.9 (Figure 5a). The 3-WL structure dominated with abundances of 45 to 81% when the system approached saturation (Figure 5b), which resulted in high p33 values that ranged from 0.56 to 0.91. Although 2-WL structures decreased with hydration, the probability of neighboring 2-WL structures remained consistently high (p22 = 0.6−0.7). The 4-WL structure location was more frequently adjacent to other thickly hydrated structures than to less-hydrated structures with p44 = 0.4−0.5 and p43 = 0.5.

Changes in WL-structure ordering were illustrated by plotting the deviation from random (R = 0) ordering for the initial dry and final saturated stages of hydration (Figure 5c,d). A positive deviation implies that the probability of a particular WL ordering was increased, whereas a negative deviation implies that the probability was decreased. Little variation from random stacking in the initial dry state occurred and layer probabilities did not exceed 0.31. A small number of systematic deviations from random were observed: positive p11 and p22 values and negative p21 and p12 values. In contrast, clearly reproducible deviations from random occurred by the final stages of apparent saturation, where enhanced probabilities for adjacent same-thickness WL structures with positive p22 values (0.2−0.64), p33 values (0.09−0.22), and p44 values (0.27−0.4) occurred. In contrast, all combinations with different adjacent WL structures were less probable. This was especially true for the probabilities that a 2-WL structure followed a

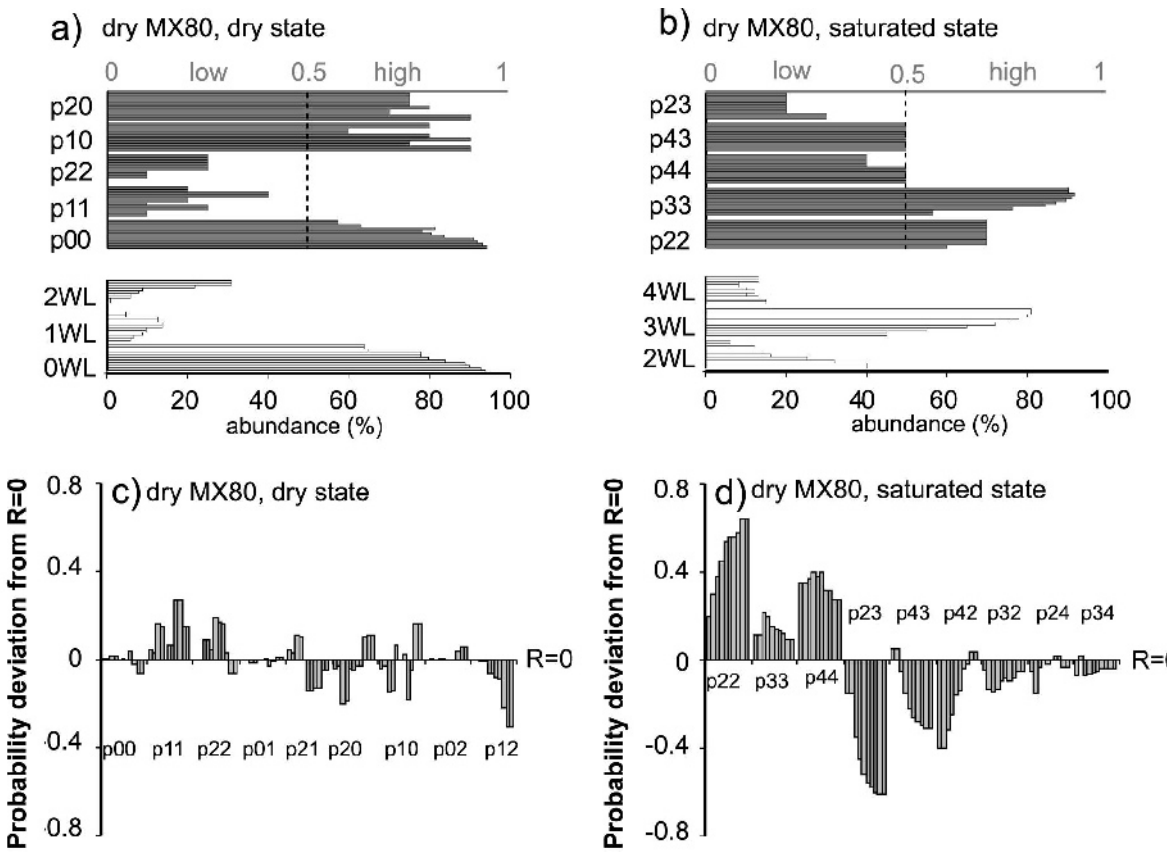

Figure 5. Ordering of mixed water-layer structures (dark gray bars) expressed as probabilities (p) and the corresponding water-layer abundance (light gray bars) for (a) dry MX80 in the initial dry state and (b) the saturated state. Ordering probabilities expressed as the deviation from the random stacking state (R=0) in the (c) dry state and (d) saturated state.

https://doi.org/10.1346/CCMN.2011.0590609 Published online by Cambridge University Press

3-WL structure (p23 = −0.15 to −0.61), a 4-WL followed a 3-WL structure (p43 = up to −0.31), and a 4-WL followed a 2-WL structure (p42 = up to −0.42). The deviations were less reproducible and were close to the zero line for other combinations, indicating random ordering. The other MX80 bentonite hydration states (moist and wet) had similar patterns with the probability of adjacent same-thickness structures always enhanced.

The patterns of increased WL ordering within particles could indicate that single aggregates of particles are hydrated around the same water-filled micro-pore. This ordering pattern does not match the distinct random (R = 0) or ordered (R = 1) character of mixed-layered hydrated Na-smectite described by Moore and Hower (1986), where smectite was hydrated by changing the relative humidity.

Quantification of water-storage sites

In addition to interlayer water quantification, determination of the relative water distributions within interlayer, external surface, and pore-storage sites during bentonite hydration was important (Figure 6). For the dry MX80 powder, total water uptake and the water adsorbed within interlayers were almost identical for the first ~2500 h, but small quantities of external water were present after 2500 h (Figure 6a). Final total water after 5040 h was 0.36 mL/g, with ~86% in interlayers (0.31 mL/g) and ~14% in external storage sites (0.05 mL/g, Table 3). The largest water proportion of 0.15 mL/g after ~310 h was external water during early-stage hydration of the moist MX80 bentonite powder (Figure 6b). This external water was most likely in pores and served as a hydration reservoir for interlayers.

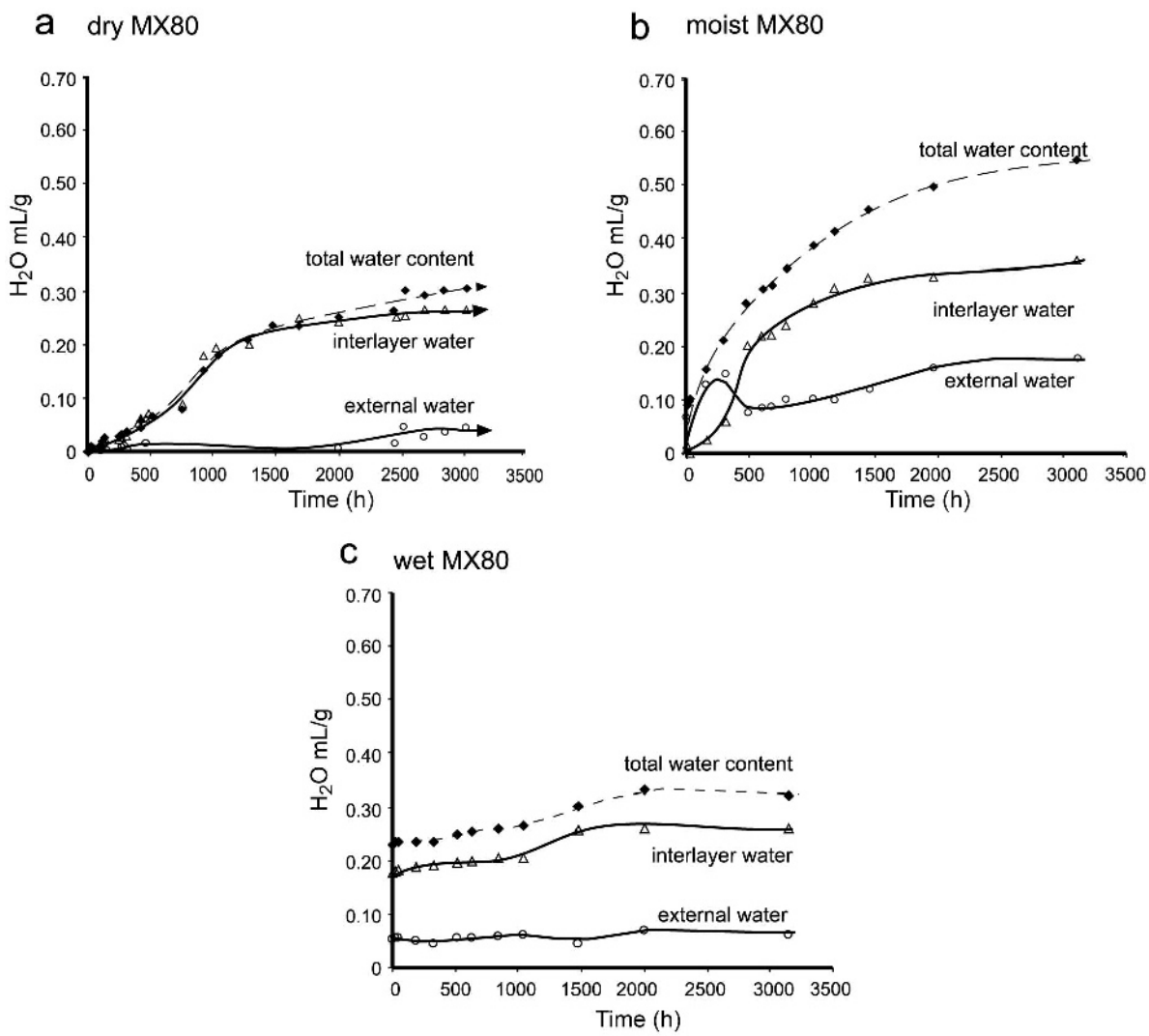

Figure 6. Water uptake into the different storage sites during hydration of MX80 bentonite of different initial hydration states and bulk densities for (a) dry, (b) moist, and (c) wet MX80. The term 'internal water' refers to the water absorbed in the interlayers; the term 'external water' refers to both surface and pore water. Data for part c from Perdrial *et al.* (2009).

https://doi.org/10.1346/CCMN.2011.0590609 Published online by Cambridge University Press

Table 4. Evolution of particle thickness and theoretical increase in accessible surface area as a function of the hydration states of MX80 bentonite.

	— Layers per stack —		Accessible surface area (m^2/g)	
	Initial	Final	Initial	Final
Dry MX80	19	7	30	81
Moist MX80	15	3	38	190

This behavior partly contradicts findings by Saiyouri *et al.* (2000) who stated that the first step in smectite hydration is always interlayer hydration, which is then accompanied by the hydration of newly accessible surfaces. After 490 h, interlayer water uptake dominated and stabilized after ~1450 h. The final amount of water adsorbed was 0.54 mL/g after 3130 h with 68% (0.36 mL/g) in interlayers and ~32% (0.18 mL/g) in external storage sites.

The wet MX80 sample contained 0.18 mL/g interlayer water and 0.05 mL/g external water prior to solution inflow (Figure 6c; Perdrial *et al*., 2009). External surface-water and pore-water contents remained relatively constant at ~0.05 mL/g and most water was in the interlayers. After 3150 h, total water was 0.32 mL/g with ~81% (0.26 mL/g) in interlayers and ~19% in external sites (0.06 mL/g).

The patterns of hydration show clearly that the storage of water in both the dry and wet MX80 samples showed similar characteristics. Both incorporated less external water than the moist MX80 sample and the storage sites were occupied in a similar way, with >80% of water stored in interlayers and <20% available as non-interlayer, external water. Such behavior indicated that a wetted bentonite powder showed equivalent sealing capacities as similarly packed dehydrated samples, though pre-hydrated bentonite will have the disadvantage of sudden volume loss and cracking when dried (Delage *et al.*, 1998; Cui *et al.*, 2002).

Accessible surface-area evolution during hydration

As commonly observed during hydration, decreased particle thickness and interlayer expansion made interlayer surfaces more accessible as layers split and detached during water uptake (Tessier, 1990). Such a mechanism would be expected to increase the accessible surface area available for adsorption. Changes in particle thickness were used to estimate theoretical changes in accessible surface area and adsorption sites. The mean particle thickness of the dry MX80 sample decreased from 19 to 7 layers, corresponding to a theoretical accessible surface area increase from 30 to 81 m^2/g (Table 4). In contrast, the mean particle thickness of moist MX80 decreased from 15 slightly hydrated layers to three layers and the accessible surface area theoretically increased from 38 m^2/g to ~190 m^2/g by the end of the experiment. This corresponds to a five-fold increase in accessible surface area when saturated. The difference between the two samples indicated that particle splitting was not as significant in the more compacted, dry MX80 sample as in the moist, less compacted sample.

Scales and mechanisms of confined-volume MX80 hydration

The results of the hydration of smectite can be visualized as a process that occurs at a variety of different sites, namely the lattice interlayers, the external surfaces of particles, and the voids between particles in single aggregates (intra-porosity) and multiple aggregates (inter-porosity; Figure 7). The effects of the confined-volume condition and the generation of swelling pressure on water storage in these sites are recognizable at a range of different scales. An influence at the lattice layer scale is visible for the sample with the lowest total and dry bulk density, the moist MX80

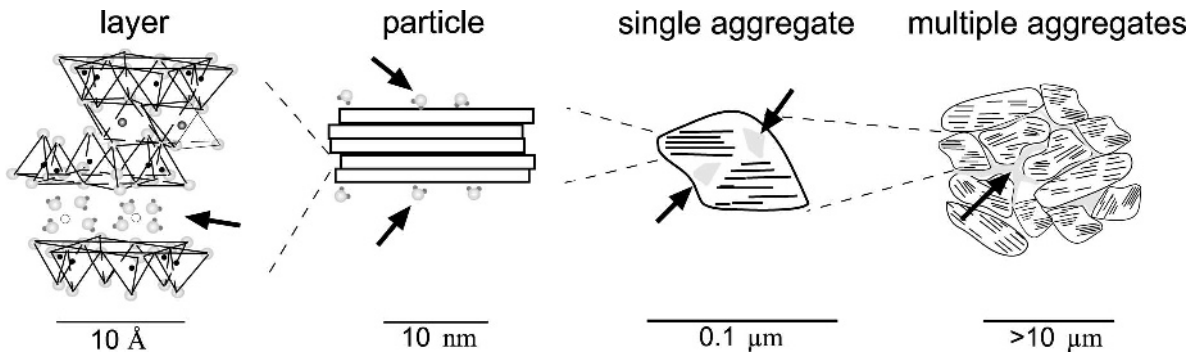

Figure 7. Different hydration sites in a smectite powder as a function of scale. Hydration sites are marked with black arrows.

https://doi.org/10.1346/CCMN.2011.0590609 Published online by Cambridge University Press

sample, which developed the thickest water-layer structures (Figure 4b). In contrast, the samples of higher bulk density (dry and wet MX80) showed a mixture of similar proportions of thinner WL structures (Figure 4a,c), indicating that the higher density suppresses thicker WL development at a layer scale (Warr and Berger, 2007; Perdrial *et al.*, 2009). The reduction in the number of 4-WL structures after 1500 h in the initially dry MX80 can similarly be attributed to the probable build up of swelling pressure in this sample. On the particle scale, the influence of the confined volume is evident from the restricted decrease in particle size and corresponding increase in accessible surface area. For example, the mean particle size of the more strongly compacted, dry MX80 decreased to only seven layers per particle, in contrast to the three layers per particle in the moist MX80 sample. A schematic reconstruction is presented (Figure 8) of the bulk-scale changes that occurred during hydration of the three different initial hydration states of MX80 bentonite leading up to saturation. The initial state refers to the samples after compaction but prior to solution inflow (Figure 8a–c). In the case of the dry MX80, the bulk texture was dominated by relatively thick particles that are closely packed; leaving only a few air-filled pores that are probably not well interconnected (Figure 8a). The relatively large inter-aggregate pores (up to 5 μm; Delage, 2007), that are strongly affected by compaction as opposed to smaller pores (>0.2 μm), are not shown (Delage and Graham, 1996; Delage and Schanz, 2007).

In contrast, particles of the moist MX80 samples were slightly thinner within a pressed powder of greater porosity, with interconnected pores that dominated the texture (Figure 8b). Because the wet MX80 sample (Figure 8c) already contained significant amounts of water, fewer air-filled pore spaces were left after the initial stages of hydration. The texture was, therefore, dominated by a decreased particle thickness with already partly hydrated interlayers and water-filled pore spaces that were, possibly but not necessarily, interconnected.

During the infiltration of solution and initial hydration, the dry MX80 sample took water in slowly and only the interlayers were hydrated. Because of the lack of interconnected pores, the hydration was likely to have proceeded as a hydration front (Figure 8d). Where water came in contact with the powder, the interlayers of the Na,Ca-montmorillonite began to hydrate. The particles adjacent to the same pore space probably took up similar amounts of water and formed aggregates with similar WL abundance. In contrast, results of the storage sites from the moist MX80 sample indicated that hydration took place *via* redistribution of pore water into the

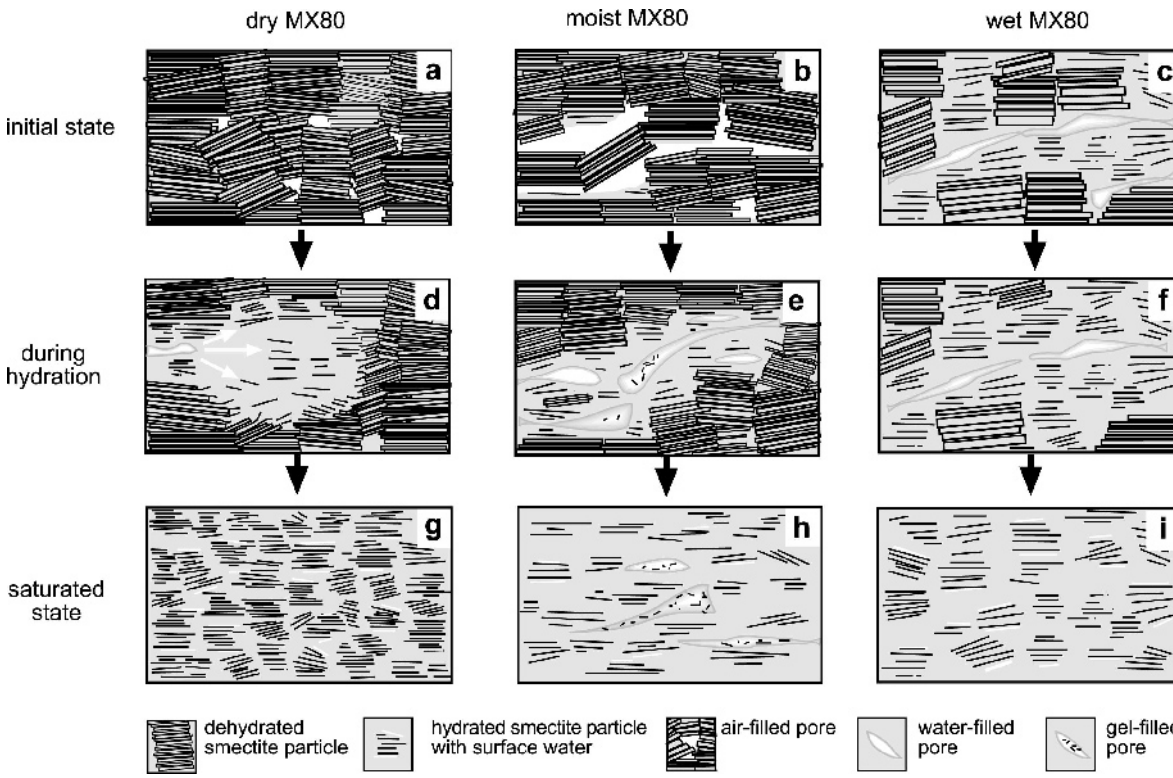

Figure 8. Schematic sketch of water uptake and hydration of smectite in confined-volume conditions (bulk textural scale) for different initial hydration states and bulk densities. (a–c) Initial stages prior to solution infiltration; (d–f) texture during hydration; and (g–i) texture at saturation.

https://doi.org/10.1346/CCMN.2011.0590609 Published online by Cambridge University Press

interlayer sites (Figure 8e). Other than in the dry and moist MX80, the wet MX80 sample did not change significantly during infiltration of solution and the amount of pore water stayed roughly the same. Only some additional interlayer hydration was observed and the particle size decreased accordingly (Figure 8f).

When the steady state was attained at the end of each experimental run, the complete saturation state was probably not attained and some isolated air-filled pores probably remained. The (initially) dry MX80 sample had the smallest water- or air-filled porosity, whereby the interlayers were well hydrated and the final particle thickness was relatively decreased (Figure 8g). The moist MX80 sample still contained important amounts of open pore spaces, probably filled with water and/or clay gels. The particle thickness had already been decreased significantly and the swelling capacity of this sample was reduced (Figure 8h). Although confined-volume studies conducted by Pusch (2001) showed that even at very high bulk densities, interconnected "external" voids can be filled with more or less dense clay gels, neither the dry nor the wet MX80 showed signs of gel formation. In the wet MX80, some pore water was present but the amount was far less significant (Figure 8i).

Implications for designing bentonite seals in underground repositories

The different methods of preparing bentonite materials currently being tested as potential backfill, *e.g.* pellets, pellet/powder mixtures, and highly compressed blocks, exhibit a range of different textures and behave differently during water saturation. In the case of compressed blocks, a system of gaps and joints occurs (Gattermann *et al.*, 2001) which acts as a water reservoir for interlayer hydration (Figure 8e). Because interlayer expansion will eventually seal the irrigation pathway, the remainder of the process should be expected to proceed by surface-controlled rates of diffusion and, therefore, be very slow. Based on the results of water-uptake rates for the different MX80 experiments, with dry bulk densities between 1.23 and 1.41 g/cm^3, the time required to saturate a 1 m thick bentonite barrier can be estimated based on the distance across the reaction cell (24 mm) and the time required to reach maximum hydration. The saturation velocities lie between ~2 and 5×10^{-9} m/s and lead to time spans of between 9.5 and almost 18 y to attain the stable state (Table 3).

In addition, the results indicated that the gaps and joints of the irrigation system may still contain gels after saturation (see Figure 8h). This point is significant because gels lead to lower hydraulic conductivity and influence the rates and mechanisms of elemental transport (Pusch, 2001; Pusch, 2006b). In contrast to smectite particles, gels are isotropic and, thus, transport becomes independent of the fabric. In the case of pellets or pellet/powder mixtures, the inter-pellet pore space should also act as reservoir sites; but, due to the greater degree of textural heterogeneity, the system may be more successful in closing these voids.

The results of this experimental study confirmed that a highly compressed dry bentonite is better than less compacted bentonite for use as backfill. Although the less compacted material in the present study revealed extensive water uptake and swelling (*e.g.* Figure 8i), note that any drying event and accompanying shrinking would result in the opening of cracks and voids that would eventually lead to the formation of pathways for circulating solutions (Montes-H. *et al.*, 2003).

CONCLUSIONS

Small-scale laboratory reaction cells can be applied successfully to confined-volume bentonite behavior using XRD techniques and can provide experimental constraints for engineering seals in underground nuclear-waste repositories. Combined with peak calculations (*CALCMIX*), specific parameters can be studied qualitatively and quantitatively to determine interlayer hydration, water distribution, WL ordering, particle thickness, and changes in accessible surface area.

Different initial hydration states and bulk densities have a large effect on water uptake and distribution into interlayer, external surface, and pore-storage sites. Water uptake by moist MX80 was greatest for the greatest dry porosity and a large proportion of external-surface water and pore water developed. Dry and wet MX80 were more densely packed, had lower dry porosities, and had significantly less external surface-water and pore-water uptake.

The ordering of WLs and particle thicknesses reflect hydration in a confined reaction volume. Greater probabilities for similar adjacent water structures might indicate that simultaneous hydration occurred around the same water-filled pores. As particle thicknesses decreased during hydration, the accessible surface area increased, but to a lesser extent than in free-swelling systems. A bulk density increase of <15% led to a decrease of >50% in the accessible surface area.

Confined-volume swelling effects on water storage sites in MX80 during hydration can be recognized at multiple scales that range from montmorillonite lattice layers to the bulk material. Different initial hydration states and bulk densities influence interlayer water thickness, the extent of particle splitting that generates new accessible surface area, and bulk changes in pore space.

Poorly to moderately packed bentonite hydration states that could be used to fill gaps in repository sites contain significant amounts of surface water and pore water during initial hydration stages. External-surface water and pore water act as reservoirs to hydrate adjacent montmorillonite particle interlayers. Some of this water might also form gel in trapped voids.

https://doi.org/10.1346/CCMN.2011.0590609 Published online by Cambridge University Press

ACKNOWLEDGMENTS

The present work was supported by the French Ministry of Research (3 year PhD grant) and the Geoparticles Group of the CGS in Strasbourg. The authors thank the anonymous reviewers and the Associate Editor for their detailed comments which significantly improved the manuscript.

REFERENCES

ANDRA (2005) Dossier 2005 – Argile, Andra, France.

Bailey, S.W. (1980) Structure of layer silicates. Pp. 1–125 in: *Crystal Structures of Clay Minerals and their X-ray Identification* (G.W. Brindley and G. Brown, editors). Monograph **5**, Mineralogical Society, London.

Bérend, I., Cases, J.M., François, M., Uriot, J.P., Michot, L., Masion, A., and Thomas, F. (1995) Mechanism of adsorption and desorption of water vapor by homoionic montmorillonites: 2. The Li+, Na+, K+, Rb+ and Cs+- exchanged forms. *Clays and Clay Minerals*, **43**, 324–336.

Bergaya, F. and Lagaly, G. (2006) General Introduction: Clays, Clay Minerals, and Clay Science. Pp. 1–18 in: *Handbook of Clay Science* (F. Bergaya, B.K.G. Theng and G. Lagaly, editors). Developments in Clay Science, **1**, Elsevier, Amsterdam.

Berger, J.N. (2008) Hydration of swelling clay and bacteria interaction – An experimental in situ reaction study. Department of Earth and Planetary Science, Strasbourg University Louis Pasteur, France, 204 pp.

Cases, J.M., Bérend, I., Besson, G., François, M., Uriot, J.P., Thomas, F., and Poirier, J.E. (1992) Mechanism of adsorption and desorption of water vapor by homoionic montmorillonite. 1. The sodium-exchanged form. *Langmuir*, **8**, 2730–2739.

Cases, J.M., Bérend, I., François, M., Uriot, J.P., Michot, L.J., and Thomas, F. (1997) Mechanism of adsorption and desorption of water vapor by homoionic montmorillonite: 3. The Mg2+, Ca2+, Sr2+ and Ba2+ exchanged forms. *Clays and Clay Minerals*, **45**, 8–22.

Chipera, S.J., Carey, J.W., and Bish, D.L. (1997) Controlled-humidity XRD analyses: application to the study of smectite expansion/contraction. Pp. 713–722 in: *Advances in X-ray Analysis*, vol. **39** (J. Gilfrich, editor). Plenum Press, New York.

Collins, D.R., Fitch, A.N., and Catlow, C.R.A. (1992) Dehydration of vermiculites and montmorillonites: a time-resolved powder neutron diffraction study. *Journal of Materials Chemistry*, **2**, 865–873.

Cui, Y.J., Yahia-Aissa, M., and Delage, P. (2002) A model for the volume change behavior of heavily compacted swelling clays. *Engineering Geology*, **64**, 233–250.

Delage, P. (2007) Microstructure features in the behaviour of engineered barriers for nuclear waste disposal. *Experimental Unsaturated Soil Mechanics*, 11–32.

Delage, P. and Graham, J. (1996) The mechanical behaviour of unsaturated soils: understanding the behavior of unsaturated soils requires reliable conceptual models. *Proceedings of the 1st International Conference on Unsaturated Soils*, Paris, Balkema, Rotterdam, pp. 1223–1256.

Delage, P., Howat, M.D., and Cui, Y.J. (1998) The relationship between suction and swelling properties in a heavily compacted unsaturated clay. *Engineering Geology*, **50**, 31–48.

Drits, V., Środoń, J., and Eberl, D. D. (1997) XRD measurement of mean crystallite thickness of illite and illite/smectite: Reappraisal of the Kübler index and the Scherrer equation. *Clays and Clay Minerals*, **45**, 461–475.

Drits, V.A., Eberl, D.D., and Środoń, J. (1998) XRD measurement of mean thickness, thickness distribution and strain for illite and illite-smectite crystallites by the Bertaut-Warren-Averbach technique. *Clays and Clay Minerals*, **46**, 38–50.

Ferrage, E., Lanson, B., Sakharov, B.A. and Drits, V.A. (2005) Investigation of smectite hydration properties by modeling experimental X-ray diffraction patterns: Part I: Montmorillonite hydration properties. *American Mineralogist*, **90**, 1358–1374.

Gattermann, J., Wittke, W., and Erichsen, C. (2001) Modelling water uptake in highly compacted bentonite in environmental sealing barriers. *Clay Minerals*, **36**, 435–446.

Grim, R.E. (1962) *Applied Clay Mineralogy.* McGraw-Hill, New York.

Hoffmann, C., Alonso, E.E., and Romero, E. (2007) Hydro-mechanical behaviour of bentonite pellet mixtures. *Physics and Chemistry of the Earth*, **32**, 832–849.

Hofman, U. and Bilke, W. (1936) Intercrystalline swelling of montmorillonite. *Kolloidzeitschrift*, **77**, 239–251.

Imbert, C. and Villar, M.V. (2006) Hydro-mechanical response of a bentonite pellets/powder mixture upon infiltration. *Applied Clay Science*, **32**, 197–209.

Johannesson, L.E., Boegesson, L., and Sandén, T. (1995) Compaction of bentonite blocks. Development of technique for industrial production of blocks which are manageable by man. SKB Technical Report, TR 95-19 Stockholm, Sweden, 48 pp.

Kahr, G., Kraehenbuehl, F., Stoeckli, H.F., and Mueller-Vonmoos, M. (1990) Study of the water-bentonite system by vapour adsorption, immersion calorimetry and X-ray techniques; II, Heats of immersion, swelling pressures and thermodynamic properties. *Clay Minerals*, **25**, 499–506.

Kaufhold, S., Dohrmann, R., and Klinkenberg, M. (2010) Water-uptake capacity of bentonite. *Clays and Clay Minerals*, **58**, 37–43.

Kraehenbuehl, F., Stoeckli, H.F., Brunner, F., Kahr, G., and Mueller-Vonmoos, M. (1987) Study of the water-bentonite system by vapour adsorption, immersion calorimetry and X-ray techniques; I, Micropore volumes and internal surface areas, following Dubinin's theory. *Clay Minerals*, **22**, 1–9.

Kühnel, R.A. and van der Gaast, S.J. (1993) Humidity controlled diffractometry and its applications. *Advances in X-ray Analysis*, **36**, 439–449.

Lagaly, G. (1993) Reaktionen des Tonminerale. Pp. 89–167 in: *Tonminerale und Tone: Struktur, Eigenschaften und Einsatz in Industrie und Umwelt* (K. Jasmund and G. Lagaly, editors). Steinkopff Verlag, Darmstadt, Germany.

Lagaly, G. (2006) Colloid clay science. Pp. 141–245 in: *Handbook of Clay Science* (F. Bergaya, B.K.G. Theng, and G. Lagaly, editors). Developments in Clay Science, vol. **1**, Elsevier, Amsterdam.

Laird, D.A., Shang, C., and Thompson, M.L. (1995) Hysteresis in crystalline swelling of smectites. *Journal of Colloid and Interface Science*, **171**, 240–245.

Likos, W.J. (2004) Measurement of crystalline swelling in expansive clay. *Geotechnical Testing Journal*, **27**, 540–546.

Likos, W.J. and Wayllace, A. (2010) Porosity evolution of free and confined bentonites during interlayer hydration. *Clays and Clay Minerals*, **58**, 399–414.

Lloret, A. and Villar, M.V. (2007) Advances on the knowledge of the thermo-hydro-mechanical behaviour of heavily compacted FEBEX bentonite. *Physics and Chemistry of the Earth*, **32**, 701–715.

MacEwan, D.M.C. and Wilson, M.J. (1980) Interlayer and intercalation complexes of clay minerals. Pp. 197–242 in: *Crystal Structure of Clay Minerals and their X-ray Identification* (G.W. Brindley and G. Brown, editors). Monograph **5**, Mineralogical Society, London.

Méring, J. (1949) L'interférence des Rayons X dans les system

à stratification désordonnée. *Acta Crystallographica*, **2**, 371–377.

Michot, L.J. and Villieras, F. (2006) Surface area and porosity. Pp. 965–978 in: *Handbook of Clay Science* (F. Bergaya, B.K.G. Theng, and G. Lagaly, editors). Developments in Clay Science, vol. **1**, Elsevier, Amsterdam.

Montes-H., G., Duplay, J., Martinez, L., and Mendoza, C. (2003) Swelling-shrinkage kinetics of MX80 bentonite. *Applied Clay Science*, **22**, 279–293.

Mooney, R.W., Keenan, A.G., and Wood, L.A. (1952) Adsorption of water vapor by montmorillonite. II. Effect of exchangeable ions and lattice swelling as measured by X-ray diffraction. *Journal of the American Chemical Society*, **74**, 1371–1374.

Moore, D.M. and Hower, J. (1986) Ordered interstratification of dehydrated and hydrated Na-smectite. *Clays and Clay Minerals*, **34**, 379–384.

Norrish, K. (1954) Crystalline swelling of montmorillonite: manner of swelling of montmorillonite. *Nature*, **173**, 256–257.

Norrish, K. and Quirk, J.P. (1954) Crystalline swelling of montmorillonite: Use of electrolytes to control swelling. *Nature*, **173**, 255–256.

Olson, K.R. (1985) Characterization of pore size distributions within soils by mercury intrusion and water-release methods. *Soil Science*, **139**, 400–404.

Perdrial, J.N., Warr, L.N., Perdrial, N., Lett, M.-C. and Elsass, F. (2009) Interaction between smectite and bacteria: Implications for bentonite as backfill material in the disposal of nuclear waste. *Chemical Geology*, **264**, 281–294.

Plançon, A. and Drits, V.A. (1999) Program for calculation of diffraction by oriented powders of two- and three-component mixed-layer clay minerals: *CALCMIX* (available from the authors).

Prost, R. (1975) Étude de l'hydratation des argiles: interactions eau-minérale et mécanisme de la rétention de l'eau. *Annales d'Agronomie*, **26**, 463–535.

Pusch, R. (2001) The microstructure of MX-80 clay with respect to its bulk physical properties under different environmental conditions. SKB Technical Report, TR-01-08 Stockholm, 108 pp.

Pusch, R. (2006a) Mechanical properties of clays and clay minerals. Pp. 247–260 in: *Handbook of Clay Science* (F. Bergaya, B.K.G. Theng, and G. Lagaly, editors). *Developments in Clay Science*, vol. **1**. Elsevier, Amsterdam.

Pusch, R. (2006b) Clays and nuclear waste management. Pp. 703–716 in: *Handbook of Clay Science* (F. Bergaya, B.K.G. Theng, and G. Lagaly, editors). *Developments in Clay Science*, vol. **1**. Elsevier, Amsterdam.

Pusch, R., Kasbohm, J., Pacovsky, J., and Cechova, Z. (2007) Are all smectite clays suitable as buffers? *Physics and Chemistry of the Earth, Parts A/B/C*, **32**, 116–122.

Saiyouri, N., Hicher, P.Y., and Tessier, D. (2000) Microstructural approach and transfer water modelling in highly compacted unsaturated swelling clays. *Mechanics of Cohesive-Frictional Materials*, **5**, 41–60.

Salles, F., Douillard, J.-M., Denoyel, R., Bildstein, O., Jullien, M., Beurroies, I., and Van Damme, H. (2009) Hydration sequence of swelling clays: Evolutions of specific surface area and hydration energy. *Journal of Colloid and Interface Science*, **333**, 510–522.

Sauzeat, E., Villiéras, T.F., François, M., Pelletier, M., Barrés, O., Yvon, J., Guillaume, D., Dubbessy, J., Pfeiffert, C., Ruck, R., and Cathelineau, M. (2001) Caractérisation minéralogique, cristallochimique et texturale de l'argile MX-80. LEM-CREGU. ANDRA Technical Report, France.

Schramm, L.L. and Kwak, J.C.T. (1982) Influence of exchangeable cation composition on the size and shape of montmorillonite particles in dilute suspension. *Clays and Clay Minerals*, **30**, 40–48.

Sposito, G. and Prost, R. (1982) Structure of water adsorbed on smectites. *Chemical Reviews*, **82**, 553–573.

Stroes-Gascoyne, S., Hamon, C.J., Maak, P., and Russel, S. (2008) The effects of the physical properties of highly compacted smectite clay (bentonite) on the culturability of indigenous microorganisms. *Applied Clay Science*, **47**, 155–162.

Tessier, D. (1990) Organisation des matériaux argileux en relation avec leur comportement hydrique. Pp. 388–445 in: *Matériaux Argileux, Structure, Propriétés et Applications* (A. Decarreau, editor). Societé Français de Minéralogie et Cristallographie, Paris.

Villar, M.V. (2007) Water retention of two natural compacted bentonites. *Clays and Clay Minerals*, **55**, 311–322.

Villar, M.V. and Lloret, A. (2007) Dismantling of the first section of the FEBEX in situ test: THM laboratory tests on the bentonite blocks retrieved. *Physics and Chemistry of the Earth*, **32**, 716–729.

Warr, L. and Berger, J. (2007) Hydration of bentonite in natural waters: Application of confined volume wet-cell X-ray diffractometry. *Physics and Chemistry of the Earth*, **32**, 247–258.

Warr, L.N. and Hofmann, H. (2003) In situ monitoring of powder reactions in percolating solution by wet-cell X-ray diffraction techniques. *Journal of Applied Crystallography*, **36**, 948–949.

Wilson, J., Cuadros, J., and Cressey, G. (2004) An in situ time-resolved XRD-PSD investigation into Na-montmorillonite interlayer and particle rearrangement during dehydration. *Clays and Clay Minerals*, **52**, 180–191.

(*Received 4 August 2010; revised 27 August 2011; Ms. 468; A.E. W.F. Jaynes*)